Resonance of flexible flapping wings at low Reynolds number

Hassan Masoud and Alexander Alexeev*
George W. Woodruff School of Mechanical Engineering, Georgia Institute of Technology, Atlanta, Georgia 30332, USA
(Received 22 September 2009; revised manuscript received 8 April 2010; published 6 May 2010)

Using three-dimensional computer simulations, we examine hovering aerodynamics of flexible planar wings oscillating at resonance. We model flexible wings as tilted elastic plates whose sinusoidal plunging motion is imposed at the plate root. Our simulations reveal that large-amplitude resonance oscillations of elastic wings drastically enhance aerodynamic lift and efficiency of low-Reynolds-number plunging. Driven by a simple sinusoidal stroke, flexible wings at resonance generate a hovering force comparable to that of small insects that employ a very efficient but much more complicated stroke kinematics. Our results indicate the feasibility of using flexible wings driven by a simple harmonic stroke for designing efficient microscale flying machines.

DOI: 10.1103/PhysRevE.81.056304 PACS number(s): 47.85.Gj, 47.32.C−, 47.63.−b

Recent rapid developments in microscale fabrication have stimulated researchers to examine the idea of designing microscale air vehicles (MAVs) that replicate flapping flight of winged insects [1–6]. To stay aloft insects generate unsteady vorticial flows [4,7–10] by flapping their extremely light, flexible wings that account for only a few percent of insect body mass [11]. Although remarkably efficient, flapping techniques used by winged insects are rather sophisticated and typically involve a combination of pitching and plunging motions [12]. Thus, the design of flapping MAVs that exactly mimic an insectlike stroke kinematics is a challenging task.

For MAV applications, it might be advantageous to design and employ wings with a simple kinematic pattern, such as a sinusoidal plunging motion. While this stroke can be more readily implemented practically, pure sinusoidal oscillations are relatively inefficient in generating lift with rigid wings. Herein, we examine how wing flexibility can be harnessed to improve the aerodynamic performance of flapping wings driven by a simple harmonic stroke. Whereas the effect of wing flexibility on flapping aerodynamics still remains unclear [13–16], it is known that certain insects employ their flexible wings at resonance [17]. This indicates that resonance regimes might improve wing performance and, therefore, could be useful for designing flapping MAVs [18–20].

We use fully coupled three-dimensional simulations to examine the low-Reynolds-number hovering aerodynamics of flexible wings oscillating at resonance. In these studies, we do not consider a complex insectlike stroke but rather focus on elastic wings driven by sinusoidal oscillations and probe how wing resonance affects aerodynamic forces at hovering. Our studies reveal that plunging wings at resonance can generate lift comparable to that of winged insects, thereby, indicating the feasibility of using flexible wings with simple stroke kinematics for designing efficient flapping MAVs.

In our simulations, we model flexible wings as flat rectangular plates plunged vertically according to a sinusoidal law. When wings are positioned normally to the oscillation plane, the symmetrical oscillations do not create a steady lift force. However, when the wings are tilted at an angle θ from the horizontal [Fig. 1(a)], the flow symmetry is broken and the wings generate lift. We show below that the proper choice of the wing's mechanical properties and tilt allows the design of plunging wings that effectively operate at a low Reynolds number Re=100.

To capture the dynamic interactions between elastic, flapping wings and a viscous fluid we employ a hybrid compu-

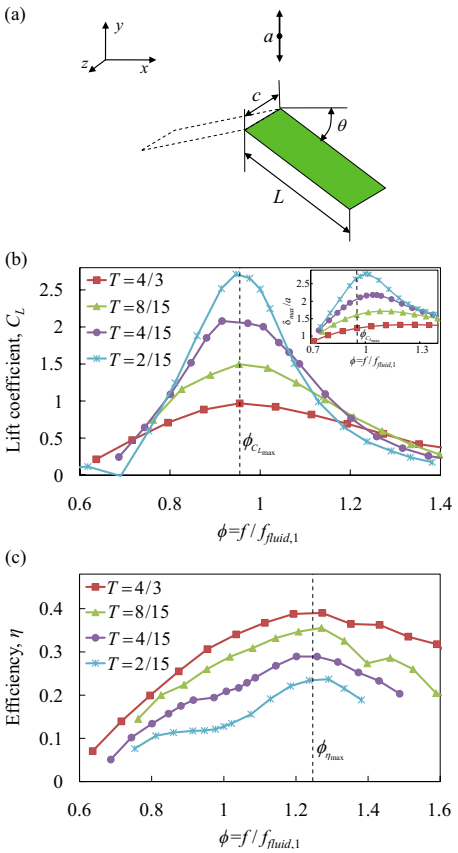

FIG. 1. (Color online) (a) Schematic of oscillating wings. The dashed line indicates the wing located beyond the symmetry plane. (b) Lift coefficient C_L and (c) flapping efficiency η versus dimensionless frequency ϕ for elastic wings with different values of the added mass parameter T. The wing tilt angle is θ=40° and Re =100. The vertical dashed lines in (b) and (c) show frequencies $\phi_{C_{L_{max}}} \approx 0.95$ and $\phi_{\eta_{max}} \approx 1.25$, respectively. The inset in (b) shows the maximum wing-tip deflection δ_{max} as a function of ϕ.

*Corresponding author; alexander.alexeev@me.gatech.edu

tational approach [21–26], which integrates the lattice Boltzmann model (LBM) for the dynamics of incompressible viscous fluids and the lattice spring model (LSM) for the mechanics of elastic solids. The two models are coupled through appropriate boundary conditions at the movable solid-fluid interface [25,27].

Briefly, the LBM is a lattice method that is based on the time integration of a discretized Boltzmann equation for particle distribution functions [28]. In three dimensions, LBM is characterized by a set of 19 distribution functions, $f_i(\mathbf{r},t)$, describing the mass density of fluid particles at a lattice node $\mathbf{r}$ and time t propagating in the direction i with a constant velocity $\mathbf{c}_i$. The hydrodynamic quantities are calculated as moments of the distribution function, i.e., the density $\rho=\Sigma_i f_i$, the momentum $\mathbf{j}=\Sigma_i \mathbf{c}_i f_i$, and the momentum flux $\Pi=\Sigma_i \mathbf{c}_i \mathbf{c}_i f_i$.

Our computational domain has dimensions $4L\times 6L\times 6L$ in the x, y, and z directions, respectively [Fig. 1(a)]. Here, L is the wing length. We use grid refinement to capture the salient features of the flow near the oscillating wing. The fine grid is localized near the wing and has dimensions $2L\times 3L\times 3L$ and lattice spacing $\Delta x_{LB}=1$ [29]. The coarse grid fills the rest of the computational domain with lattice spacing $\Delta x_{LBc}=2$ and is coupled with the fine grid using the volumetric formulation [30].

The elastic wings are modeled via the LSM that represents the solid material as a network of harmonic springs connecting lattice nodes. Since the thickness of the wing is much smaller than its other dimensions, we use a two-dimensional triangular lattice with stretching and bending springs characterized by spring constants k_s and k_b, respectively. The stretching springs connect neighboring nodes and give rise to in-plane stiffness, whereas the bending springs incorporate the interactions between consecutive pairs of nodes and account for the wing's bending rigidity. With this spring arrangement, the solid material is characterized by the Poisson's ratio $\nu=1/3$ and the bending modulus $EI=\frac{3\sqrt{3}}{4}k_b c(1-\nu^2)$, where E is the Young's modulus and $I=cb^3/12$ is the moment of inertia with c and b being the chord and thickness of the rectangular wing, respectively. In our simulations, we vary k_b to modify the wing bending properties.

We use the velocity Verlet algorithm to integrate Newton's equation of motion for the lattice nodes, $\mathbf{F}(\mathbf{r}_i)=m(d^2\mathbf{r}_i/dt^2)$, where $\mathbf{F}$ is the total force acting on the node with mass $m=\frac{\sqrt{3}}{2}\rho_s b\Delta x_{LS}^2$ at position $\mathbf{r}_i$. Here, ρ_s is the solid density and Δx_{LS} is the lattice spacing. The total force includes the force due to the interconnecting springs and the force exerted by the fluid at the solid-fluid interface [23,25,31].

The flexible wing is formed from 23×11 LSM nodes with $\Delta x_{LS}=2.325$, yielding the wing sizes $L=50$ and $c=0.4L$ [Fig. 1(a)]. Two rows of nodes are placed beyond the symmetry boundary at $x=0$ and serve to impose the wing vertical oscillations with an amplitude $a=0.2L$. At the rest of the outer boundaries, we apply the no-flow condition. Thus, we effectively model a pair of simultaneously oscillating wings with a symmetry plane at $x=0$. We set the flapping frequency f such that wing oscillations yield a Reynolds number $\mathrm{Re}=2\pi fac/\nu$ equal to 100. For the fluid properties, we set the density $\rho=1$ and the kinematic viscosity $\nu=2.5\times 10^{-3}$.

We have previously validated our model in the limit of $\mathrm{Re}\ll 1$ [23,25,31] and showed that the coupled model is of second-order accuracy in the spatial resolution [25]. Here, we further tested the model by simulating three-dimensional flows around rectangular wings at $\mathrm{Re}=100$. When compared with the experimental data, we found good agreement with respect to drag and lift coefficients with errors less than 5% [32]. We also calculated the drag coefficient on a plate oscillating at low Re ranging from 100 to 750. These results were found in excellent agreement with previously reported experiments [33,34]. To assess the grid quality, we applied fine grid for the entire computational domain and doubled the domain size. In both these tests, the difference in the drag and lift coefficients between the simulations did not exceed 3%. We also verified that the LSM grid is sufficiently accurate to capture the dynamic deformations of the elastic wing.

The wing dynamic response to aerodynamic loads is defined by the wing geometry and material properties. In addition to Re, we characterize the flexural oscillations of the elastic wing in terms of the dimensionless frequency $\phi=f/f_{fluid,1}$ and the parameter $T=\rho c/\rho_s b$ that indicates the ratio between added and apparent masses. Here, $f_{fluid,1}$ is the fundamental resonance frequency in viscous fluid, which is found from the linear theory of small amplitude oscillations of high-aspect-ratio elastic beams, i.e., $a\ll c\ll L$ [35]. Note that $f_{fluid,1}$ is a function of Re, T, and EI [35].

We characterize the wing performance by the lift coefficient $C_L=2\bar{F}_y/cLU_0^2$ and the wing efficiency $\eta=C_L/C_p$, where $C_p=2P/cLU_0^3$ is the power coefficient. Here, $\bar{F}_y$ is the vertical component of a period-averaged hydrodynamic force on the oscillating wing, P is the power required for flapping the wing during one period, and $U_0=2\pi af$ is the characteristic velocity of wing oscillations.

In Fig. 1(b), we plot the lift coefficient C_L as a function of the dimensionless frequency ϕ for wings tilted at $\theta=40°$ and different added mass parameters T. When tilted elastic wings oscillate at frequencies within the resonance band, the bending amplitude increases [see inset in Fig. 1(b)]. This may enhance the lift generation. Indeed, the lift coefficient increases significantly at resonance and reaches the maximum at $\phi_{C_{L\,\max}}\approx 0.95$ for all T. It is rather surprising that a linear theory can be used for predicting the frequency of the maximum lift coefficient $C_{L\,\max}$; in our simulations $a=0.5c$ and $c=0.4L$, which are clearly beyond the limits of applicability of the theoretical model [35]. It is also noteworthy that $\phi_{C_{L\,\max}}$ does not coincide with the frequency of the maximum wing-tip deflection.

We found that $C_{L\,\max}$ is greater for wings with smaller T for which the effect of wing inertia is more pronounced. However, even for the lightest wings considered in our studies, for which the maximum tip deflections $\delta_{\max}$ is about a [see inset in Fig. 1(b)], the maximum lift force is about 100 times greater than the lift force produced by tilted rigid wings with identical geometry driven by a sinusoidal stroke with amplitude a, in which case $C_{L\,\max}\approx 0.02$. This result indicates that the wing elastic deformations are critical for

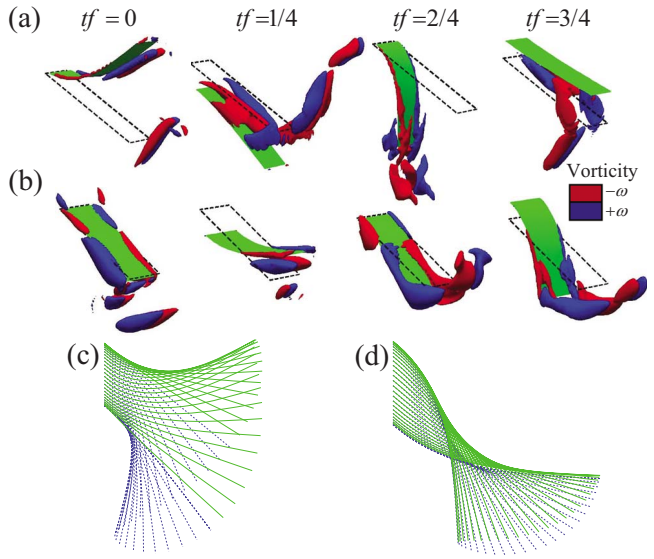

FIG. 2. (Color online) Snapshots in panels (a) and (b) illustrate the elastic deformations and vorticial flows arising around flexible wings oscillating at $\phi_{C_{L_{\max}}}$ and $\phi_{\eta_{\max}}$, respectively. Color surfaces (dark gray) indicate the isovorticial surfaces with the vorticity magnitude $\omega=8f$ in (a) and $\omega=2f$ in (b). The dashed contours in (a) and (b) show the initial position of an undeformed wing. Panels (c) and (d) show wing profiles for, respectively, $\phi_{C_{L_{\max}}}$ and $\phi_{\eta_{\max}}$. The profiles for downstroke are shown by the solid green lines, whereas the upstroke profiles are shown by the dashed blue lines. The wing parameters are $\theta=40°$, $T=2/15$, and Re=100.

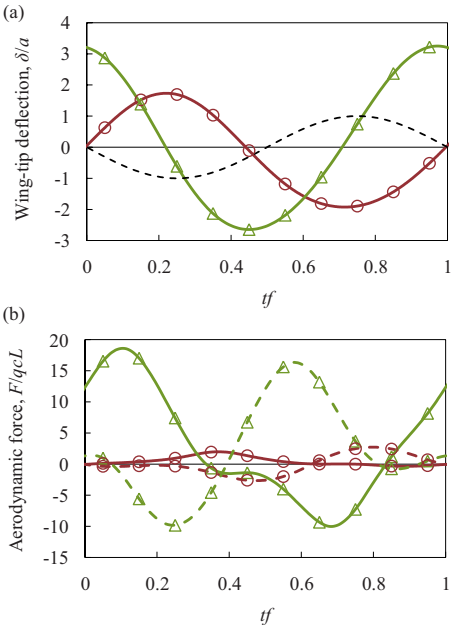

FIG. 3. (Color online) (a) Wing-tip deflection and (b) aerodynamic forces during one period of wing oscillations. The triangle and circle symbols are for $\phi=\phi_{C_{L_{\max}}}$ and $\phi=\phi_{\eta_{\max}}$, respectively. In (a), the dashed line indicates the wing root position. In (b), the solid and dashed lines show, respectively, the vertical and horizontal components of aerodynamic force on the oscillating flexible wing. The wing parameters are $\theta=40°$, $T=2/15$, and Re=100.

enhancing aerodynamic lift at resonance. We conclude that resonance oscillations are preferable for producing aerodynamic lift using wings driven by a simple harmonic stroke.

Not only lift but also the aerodynamic efficiency of flapping wings is greatly enhanced at resonance frequencies [Fig. 1(c)]. We found that the maximum efficiency $\eta_{\max}$ increases with increasing T and almost doubles when T changes from 4/30 to 4/3. This is in contrast to $C_{L\,\max}$ which decreases with increasing T [Fig. 1(b)]. For all T considered in our simulations, we found that $\eta_{\max}$ takes place at $\phi_{\eta_{\max}} \approx 1.25$ and, therefore, $\phi_{\eta_{\max}}/\phi_{C_{L\,\max}} \approx 1.3$. Thus, by changing the oscillation frequency between $\phi_{C_{L\,\max}}$ and $\phi_{\eta_{\max}}$, the wing performance can be tuned to the regimes leading to the maximum lift and efficiency, respectively. Furthermore, we found that $\eta_{\max}$ of flexible wings significantly exceeds the maximum efficiency of otherwise identical rigid wings equal to 0.01.

To gain insight into the wing aerodynamics at $\phi_{C_{L\,\max}}$ and $\phi_{\eta_{\max}}$, we present in Fig. 2 a series of snapshots illustrating wing elastic deformations and emerging vorticial flows [36]. For $\phi=\phi_{C_{L\,\max}}$ [Fig. 2(a)], the flexible wing induces two basic vortices along the opposite wing edges. In this regime, the wing tip oscillates with a phase lag of $\pi/2$ relative to the root [see Fig. 3(a)]. When wing moves downwards, the combination of the inertial forces and fluid drag bends the wing up such that its surface is roughly normal to the direction of motion [see Fig. 2(a) for $tf=0$ and Fig. 2(c)]. This enhances aerodynamic forces experienced by the flexible wing during downstroke. During the upward stroke, the wing bends toward the vertical axis and slides over the vortices created during downstroke [see Fig. 2(a) for $tf=2/4$], thus reducing the aerodynamic resistance. The asymmetry between the downstroke and upstroke gives rise to the net lift generated by the wing. The driving amplitude a while not affecting the resonance frequency sets the magnitude of the relative displacement of the deformed wing during the downstroke and upstroke and, in this way, controls the magnitude of the net lift force.

Figures 2(b) and 2(d) show an elastic wing oscillating at $\phi=\phi_{\eta_{\max}}$. In this regime, the wing tip and root move with a phase shift of π relative to each other [Fig. 3(a)]. As a result of this out-of-phase motion, the wing does not exhibit a significant displacement at $L/2$ but rather "rotates" around this nodal line separating the inner and outer wing sections that effectively oscillate in counterphase [Fig. 2(d)]. That is when the inner section moves downwards, the outer section moves upwards and vice versa. The out-of-phase oscillations generate two separated pairs of vortices with opposite rotations, which are located along the edges of the two wing sections [see Fig. 2(b) for $tf=0$ and 2/4] and evolve in time in a fashion similar to that of vortices at $\phi=\phi_{C_{L\,\max}}$.

The frequency change between $\phi_{C_{L\,\max}}$ and $\phi_{\eta_{\max}}$ not only affects the phase of wing tip oscillations [Fig. 3(a)] but also alters the instantaneous aerodynamic forces experienced by the wing. In Fig. 3(b), we show the time evolution of horizontal F_x and vertical F_y components of the aerodynamic force. At frequency $\phi_{C_{L\,\max}}$, both the horizontal and vertical forces exhibit similar profiles with a phase shift of π relative to each other. A nonzero period-averaged F_y gives rise to the

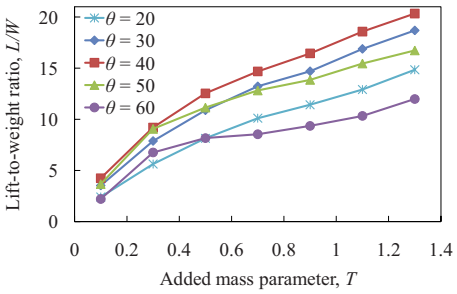

FIG. 4. (Color online) Lift-to-weight ratio L/W versus added mass parameter T for a 5 mm flexible wing oscillating in air with frequency $\phi=\phi_{C_{L_{\max}}}$ and Re=100.

lift force $\bar{F}_y$, whereas the period-averaged horizontal force $\bar{F}_x$ creates side flows that transport the vortices away from the wing [see Fig. 2(a) for $tf=1/4$].

At $\phi=\phi_{\eta_{\max}}$, the vertical force F_y is directed upward for the entire oscillation period and its fluctuations are relatively small [Fig. 3(b)]. This behavior is a consequence of the paired vorticial structure emerging at $\phi_{\eta_{\max}}$ that distributes the aerodynamic load more uniformly between the inner and outer wing sections. Compared to $\phi_{C_{L\,\max}}$, fluctuations of F_y at $\phi_{\eta_{\max}}$ decrease from 5.2 to 2.6 relative to the average value. Furthermore, $\bar{F}_x$ is practically nil in this regime, and thus, the wing produces relatively weak flows normal to the oscillation plane. The later seems to contribute to overall greater efficiency at $\phi_{\eta_{\max}}$ where the vortices stay localized near the flapping wing.

When it comes to designing MAVs, an important parameter is the ratio between the lift generated by a wing and the wing's weight L/W. This ratio indicates the amount of load that could be carried by a winged flyer. For insects, this ratio is typically greater than 20 [11]. In Fig. 4, we plot L/W as a function of T for 5 mm wings with different tilt angle θ, oscillating in the air with a frequency of $f\approx 125$ Hz. We set the wing elasticity such that $\phi=\phi_{C_{L\,\max}}$. We found that L/W is maximum at $\theta=40°$, which is also the optimum angle for lift generation. More importantly, L/W significantly exceeds unity and, for larger T, approaches the values typical for insects. In other words, plunging elastic wings at resonance can lift loads many times heavier than their own weight. There are, however, limitations to the practical values of T imposed by the mechanical properties of materials. Typical polymer density is about $\rho_s\sim 1000\rho$, in which case a wing with rectangular cross-section and $T=1$ yields the thickness $b\approx 2$ μm and the bending rigidity $EI\approx 10^{-10}$ N m^2, leading to the modulus $E\approx 75$ GPa. These parameters are still in the range of experimentally realistic values [37]; however the use of wings with larger T may require the development of new materials with enhanced modulus [38].

In summary, we used three-dimensional computational modeling to examine the hovering aerodynamics of flexible plunging wings at Re=100. Our simulations revealed that at resonance tilted elastic wings driven by a simple harmonic stroke generate lift comparable to that of small insects that employ a significantly more complex stroke [4,11,12,39]. Such simple oscillations can be more readily adapted for designing flapping MAVs. Furthermore, we showed that just by changing wing elasticity, the lift force can be increased by two orders of magnitude indicating the drastic effect that elasticity may play in flapping flight. We found that elastic wings at resonance yield a high lift-to-weight ratio and efficiency. We identified two oscillation regimes leading to different wing bending modes that maximize the lift and efficiency, respectively. These two regimes take place at frequencies that differ by approximately 30%. Therefore, they can be dynamically changed by altering the flapping frequency. This could be useful for regulating the flight of flapping-wing MAVs since high lift is typically needed only during takeoff, while the improved aerodynamic efficiency is essential for a long-distance cruise flight.

Finally we note that in the present studies, we focused on the hovering flight with flexible wings at resonance. To employ the resonance flapping in practical MAV applications it will be necessary to examine how this approach can be adapted for thrust generation in forward flight and how the resonant wings behave and can be effectively controlled in different flow conditions including unsteady gusty environments. With respect to the former, a thrust force can be generated by using flapping wings with a nonzero angle of incidence. Furthermore, here we examined flexible wings with a fixed aspect ratio and uniform mechanical properties. Although these simple wings could be more readily manufactured, the use of wings with an optimized geometry, nonuniform structural and anisotropic mechanical properties, and asymmetric stroke kinematic may further enhance the resonance performance of flapping wings. These studies are currently underway.

This work was supported in part by the NSF through TeraGrid computational resources.

[1] C. P. Ellington, J. Exp. Biol. **202**, 3439 (1999).
[2] S. A. Ansari, R. Zbikowski, and K. Knowles, Prog. Aerosp. Sci. **42**, 129 (2006).
[3] R. Zbikowski, Philos. Trans. R. Soc. London, Ser. A **360**, 273 (2002).
[4] W. Shyy, Y. Lian, J. Tang, H. Liu, P. Trizila, B. Stanford, L. Bernal, C. Cesnik, P. Friedmann, and P. Ifju, Acta Mech. Sin. **24**, 351 (2008).
[5] R. J. Wood, IEEE Trans. Rob. Autom. **24**, 341 (2008).
[6] R. S. Fearing and R. J. Wood, in *Flying Insects and Robots* (Springer, Heidelberg, 2009), pp. 219–229.
[7] M. H. Dickinson, F. O. Lehmann, and S. P. Sane, Science **284**, 1954 (1999).
[8] S. P. Sane, J. Exp. Biol. **206**, 4191 (2003).
[9] F. O. Lehmann, J. Exp. Biol. **211**, 224 (2008).
[10] U. Pesavento and Z. J. Wang, Phys. Rev. Lett. **103**, 118102

(2009).
[11] C. P. Ellington, Philos. Trans. R. Soc. London, Ser. B **305**, 17 (1984).
[12] C. P. Ellington, Philos. Trans. R. Soc. London, Ser. B **305**, 41 (1984).
[13] J. Young, S. M. Walker, R. J. Bomphrey, G. K. Taylor, and A. L. R. Thomas, Science **325**, 1549 (2009).
[14] P. Rojratsirikul, Z. Wang, and I. Gursul, Exp. Fluids **46**, 859 (2009).
[15] M. Bozkurttas, R. Mittal, H. Dong, G. V. Lauder, and P. Madden, J. Fluid Mech. **631**, 311 (2009).
[16] W. Shyy, Y. Lian, S. K. Chimakurthi, J. Tang, C. E. S. Cesnik, B. Stanford, and P. G. Ifju, *Flying Insects and Robots* (Springer, Heidelberg, 2009), pp. 143–157.
[17] R. Dudley, Annu. Rev. Physiol. **62**, 135 (2000).
[18] L. Liu, Z. Fang, and Z. He, *Intelligent Robotics and Applications* (Springer, Heidelberg, 2008), pp. 245–255.
[19] M. Vanella, T. Fitzgerald, S. Preidikman, E. Balaras, and B. Balachandran, J. Exp. Biol. **212**, 95 (2009).
[20] S. Michelin and S. G. L. Smith, Phys. Fluids **21**, 071902 (2009).
[21] R. Ghosh, G. A. Buxton, O. B. Usta, A. C. Balazs, and A. Alexeev, Langmuir **26**, 2963 (2010).
[22] H. Masoud and A. Alexeev, Soft Matter **6**, 794 (2010).
[23] A. Alexeev, R. Verberg, and A. C. Balazs, Phys. Rev. Lett. **96**, 148103 (2006).
[24] K. A. Smith, A. Alexeev, R. Verberg, and A. C. Balazs, Langmuir **22**, 6739 (2006).
[25] A. Alexeev, R. Verberg, and A. C. Balazs, Macromolecules **38**, 10244 (2005).
[26] A. Alexeev and A. C. Balazs, Soft Matter **3**, 1500 (2007).
[27] M. Bouzidi, M. Firdaouss, and P. Lallemand, Phys. Fluids **13**, 3452 (2001).
[28] S. Succi, *The Lattice Boltzmann Equation for Fluid Dynamics and Beyond* (Oxford University Press, Oxford, 2001).
[29] All dimensional values are given in lattice Boltzmann units, if not stated otherwise.
[30] H. Chen, O. Filippova, J. Hoch, K. Molvig, R. Shock, C. Teixeira, R. Zhang, Physica A **362**, 158 (2006).
[31] A. Alexeev, R. Verberg, and A. C. Balazs, Langmuir **23**, 983 (2007).
[32] K. Taira and T. Colonius, J. Fluid Mech. **623**, 187 (2009).
[33] C. C. Shih and H. J. Buchanan, J. Fluid Mech. **48**, 229 (1971).
[34] G. H. Keulegan and L. H. Carpenter, J. Res. Natl. Bur. Stand. **60**, 423 (1958).
[35] C. A. Van Eysden and J. E. Sader, J. Appl. Phys. **101**, 044908 (2007).
[36] See supplementary material at http://link.aps.org/supplemental/10.1103/PhysRevE.81.056304 for movies illustrating the resonance oscillations of a flexible wing.
[37] J. Brandrup, E. H. Immergut, and E. A. Grulke, *Polymer Handbook*, 4th ed. (Wiley, New York, 1999).
[38] The use of structured and/or composite wings could significantly increase the bending rigidity and therefore reduce the required material modulus.
[39] Z. J. Wang, Annu. Rev. Fluid Mech. **37**, 183 (2005).